

False Data Injection Attacks on Hybrid AC/HVDC Interconnected System with Virtual Inertia – Vulnerability, Impact and Detection

Kaikai Pan*, Elyas Rakhshani, and Peter Palensky

Abstract—Power systems are moving towards hybrid AC/DC grids with the integration of HVDC links, renewable resources and energy storage modules. New models for frequency control have to consider the complex interactions between these components. Meanwhile, more attention should be paid to cyber security concerns as these control strategies highly depend on data communications which may be exposed to cyber attacks. In this article, for the first time, we study the false data injection attacks on the hybrid AC/DC grid with virtual inertia. We then build an optimization-based framework for vulnerability and impact analysis. It is shown that the hybrid grid with inertia emulation capability is more vulnerable to the false data injection attacks, compared with the normal AC system. We also propose a detection approach to detect and isolate each intrusion, and even recover the attack value in the steady-state behavior. In addition to theoretical results, the effectiveness of the proposed methods is validated through simulations on the two-area AC/HVDC interconnected system.

Index Terms—hybrid AC/HVDC system, inertia emulation, frequency control, false data injection attacks

I. INTRODUCTION

RECENT advances in power electronics have made HVDC links and renewable energy resources (RES) more popular in modern power system applications [1]. For better support of frequency control, the recent research tries to come up with different approaches for inertia emulation tasks [2]. This transformation does not only lead to more adaption of conventional control strategies such as automatic generation control (AGC) to handle complex interactions in the hybrid AC/HVDC grid but also introduce an increasing dependence on data communications. The AGC of tomorrow must consider new AC/DC multi-area systems incorporating virtual inertia controllers [3]. Besides, it would also rely on communication networks and numerous cyber devices to achieve reliable and in-time data exchange. However, the wide communication surface of the AC/DC power grid with virtual inertia makes them more exposed to cyber threats, including false data injection (FDI) attacks [4]. Notably, as we know, the DC grid has a low tolerance to a fault; if a single fault can mislead a fast response, so as an attack. Indeed, a deliberate attacker can result in severe consequences on system instability [5]. Thus one need advanced tools to understand the attacks and also address them in the AC/DC interconnected system which is facilitated by virtual inertia emulators.

Related work: Nowadays, the matter of virtual inertia is one of the hottest topics in the power system studies [6], [7]. New models of frequency control have been proposed for the integration of RES by using Energy Storage Systems (ESS) [8]. In the AC/DC interconnected systems, these components need to be coordinated under the AGC operation, which also highlights the importance of cyber-secure data communications [9]. We can see that much work has been done on the cyber security research of pure AC power systems. Vulnerability and impact analysis of the AC grids to cyber attacks can be found in [10], [11]. Model-based detection methods to reveal FDI attacks have also emerged mainly from observer-based approaches under linear differential-algebraic equations (DAEs) [12]. For instance, in [13] an unknown input observer was employed in detecting FDI attacks on the AC system. Other detection techniques come from statistical methods which usually have prior assumptions on the distribution of measurement errors [14].

For the hybrid AC/HVDC grid with inertia emulation capability, however, there are very few studies have focused on its cyber security research [15]. To do that, it requires both extensive knowledge on the complex AC/DC system with virtual inertia and advanced methods or algorithms from the cyber security domain. In reference [16], the impact of cyber attacks on the HVDC transmission oscillation damping control was explored. The latest work in [17] studied the effect of attacks on the HVDC system and its impact on the dynamic voltage stability and switching power losses. However, there is a still huge gap here especially for the research on the frequency dynamics of the hybrid system with virtual inertia under cyber attacks. To the best of our knowledge, the following question is still not answered sufficiently,

Is it possible to quantify the vulnerability and impact of FDI attacks on the AC/HVDC interconnected system with virtual inertia, and propose advanced diagnosis tools to reveal the malicious intrusions?

Our contributions: In this article our aim to address the question above. For this purpose, we would first build up the system model of the hybrid AC/DC grid with ESS for providing virtual inertia. A high-level control strategy is presented, which also illustrates possible vulnerable points of the grid to FDI attacks. Next, we introduce impact indices to evaluate the effect of FDI attacks on dynamic frequency stability. We formulate an optimization-based framework to assess the vulnerability of the grid to possible disruptive

The authors are with the Delft University of Technology, The Netherlands.
(* Correspondence: K.Pan@tudelft.nl)

stealthy attacks. Afterwards, a detector in the form of residual generator is proposed to detect, isolate and even recover each FDI attack. The main contributions of this article are:

- (i) Unlike the existing literature, we go beyond the study on the normal AC grid that for the first time we explore the vulnerability and impact of the hybrid AC/HVDC grid with virtual inertia to the FDI attacks. A well-constructed optimization framework is built to analyze the attack strategies on achieving undetectability and desired impact. From both the theoretical analysis and numerical results, we have pointed out that the hybrid grid with inertial emulation capability can be more vulnerable to FDI attacks, compared with the AC/DC grid without virtual inertia and the normal AC grid.
- (ii) We further explore the attack detection problem in the hybrid grid. Note a low-order detector is more desired for online implementation in reality. Thus different from observer-based approaches which usually have the same degrees with the system dynamics, we formulate a type of residual generator that can have much lower order. It is also guaranteed that the resulting residual signal is decoupled from the system states and disturbance, and can recover the attack value in the steady-state behavior. We also provide attack isolation method together with conditions of attack detectability and isolability.

In Section II, we describe the system model and the high-level control strategy of the hybrid AC/DC grid with virtual inertia. Section III introduces the FDI attack and its optimal strategy to be disruptive and stealthy. We also propose an optimization framework to analyze the vulnerability of the grid to such attacks. The attack detection approach is presented in Section IV where we also show its capabilities of attack isolation and recovery. Numerical simulations are in Section V.

II. HYBRID AC/HVDC-ESS SYSTEM MODELING

In this section, a high-level control model is presented to simulate and analyse the behaviour of the AC/DC transmission system with the ability of inertia emulation.

A. The concept of virtual inertia

For the inertia emulation task, one effective way is to use the derivation of the system frequency proportionally to adjust the active power reference of a converter. Then the emulated inertia can contribute to improve the performance of the system dynamics on the inertia response. This control concept is the derivative control which calculates the rate of change of frequency (ROCOF) [18], and can be described as,

$$\Delta P_{emu} = k_a \omega_o \Delta \dot{\omega}, \quad (1)$$

where ΔP_{emu} is the power reference, k_a is the inertial proportional conversion gain and ω_o is the nominal frequency.

B. Modeling of AC/DC system with virtual inertia capability

The diagram of an exemplary two-area AC/DC interconnected grid with added bulk ESS for providing virtual inertia

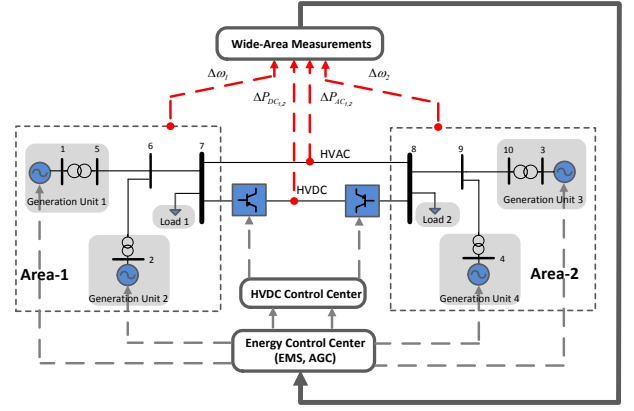


Figure 1: The two-area interconnected system with ESS and parallel AC/DC links. To be illustrative, the wide-area frequency and AC/DC power flow measurements are vulnerable to FDI attacks. EMS: energy management system.

is presented in Figure 1. In this test system, two converters are added as interfaces for controlling the behavior of the ESS modules in accordance with AGC control signals to reduce the deviations of system frequency. As depicted in Figure 1, wide-area frequency and AC/DC power flow measurements are collected in each area and tie-line, and sent to the control center via communication networks for the AGC operation, HVDC coordination and inertia emulation. We illustrate the high-level control structure of the parallel AC/DC link in co-ordination with derivative control of ESS for inertia emulation in Figure 2. According to this control strategy, the frequency variation in the Laplace domain can be obtained,

$$\Delta \omega_i(s) = \frac{K_{p_i}}{1 + sT_{p_i}} [\Delta P_{m_i} - \Delta P_{L_i} - (\Delta P_{AC_{i,j}} + \Delta P_{DC_{i,j}} + \Delta P_{ESS_i})], \quad (2)$$

where ΔP_{ESS_i} and ΔP_{m_i} are the emulated power from ESS and the total active power from all generation units (GENs) within Area i , i.e., $\Delta P_{m_i} = \sum_{g=1}^{G_i} \Delta P_{m_{i,g}}$ where G_i denotes the number of participated GENs. K_{p_i} is the system gain and T_{p_i} is the system time constant. The load variation is mentioned by ΔP_{L_i} , while $\Delta P_{AC_{i,j}}$ is the AC power flow deviation and $\Delta P_{DC_{i,j}}$ denotes the DC power. We can have

$$\Delta P_{m_{i,g}}(s) = \frac{1}{1 + sT_{ch_{i,g}}} \left[\frac{\Delta \omega_i}{R_{i,g} \times 2\pi} - \phi_{i,g} \Delta P_{agc_i} \right], \quad (3)$$

$$\Delta P_{AC_{i,j}}(s) = \frac{T_{ij}}{s} [\Delta \omega_i - \Delta \omega_j]. \quad (4)$$

In the equations above, $R_{i,g}$ denotes the droop of each generation unit. $T_{ch_{i,g}}$ is the overall time constant of the turbine-governor model. ΔP_{agc_i} is the signal from AGC output of Area i for power reference of each generation unit, and $\phi_{i,g}$ is its area participating factor in the AGC. T_{ij} denotes the power coefficient of the AC line between these two areas.

To model the HVDC link, we use the concept of Supplementary Power Modulation Controller (SPMC). As illustrated in Figure 2, the SPMC can be designed as a high-level damping controller whose inputs consist of deviations of frequencies in

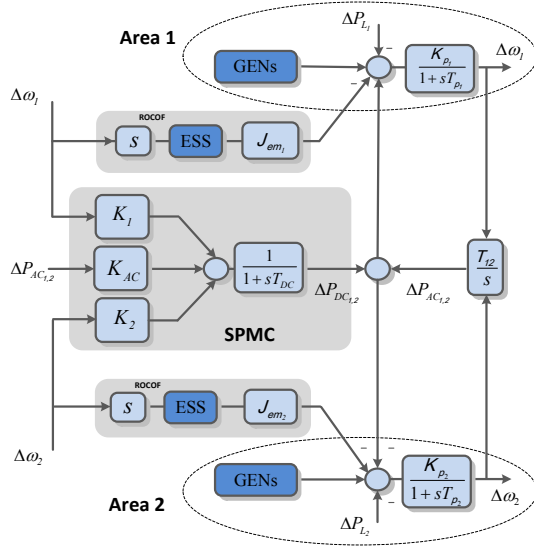


Figure 2: High-level control structure of the two-area hybrid AC/DC system with virtual inertia based on [18].

the interconnected areas and the deviation of the transmitted power in the parallel AC line. Then the output of SPMC is used for the DC link to generate the desired DC power. Thus the coordinated control strategy acting as a supplementary power modulation for this HVDC link can be expressed as:

$$\Delta P_{DCref} = K_i \Delta \omega_i + K_j \Delta \omega_j + K_{AC} \Delta P_{ACi,j}, \quad (5)$$

$$\Delta P_{DCi,j}(s) = \frac{1}{1 + sT_{DC}} \Delta P_{DCref}, \quad (6)$$

where ΔP_{DCref} denotes the control signal for the HVDC line (the desired DC power reference), T_{DC} is the time constant of the DC link, and K_i , K_j and K_{AC} are used as control gains.

For the inertia emulation process, according to Section II-A, the deviation of active power output from the ESS in each area (ΔP_{ESS_i}) can be written as:

$$\Delta P_{ESS_i}(s) = \frac{J_{em_i}}{1 + sT_{ESS_i}} [s \Delta \omega_i(s)], \quad (7)$$

where T_{ESS_i} is the time constant of the derivative-based components. There will be two gains (J_{em_1} and J_{em_2}) representing the virtual inertia for these two areas; see Figure 2.

The part of AGC control calculates the Area Control Error (ACE) of Area i . The ACE signal now contains the frequency of that area and both AC/DC power flow deviations, and acts as inputs for an integral control action,

$$ACE_i = \frac{\beta_i}{2\pi} \Delta \omega_i + (\Delta P_{ACi,j} + \Delta P_{DCi,j}), \quad (8)$$

$$\Delta P_{agc_i} = K_{I_i} \frac{ACE_i}{s}, \quad (9)$$

in which β_i is the frequency bias and K_{I_i} represents the integral gain of the AGC controller. Thus finally, based on the equations (2) to (9), the system model of the exemplary

two-area AC/DC network with virtual inertia can be presented as the state equation,

$$\dot{X}(t) = A_c X(t) + B_{c,d} d(t). \quad (10)$$

where $X \in \mathbb{R}^{n_x}$ represents the vector of all state variables, and $d \in \mathbb{R}^{n_d}$ is the system input related to load changes, namely,

$$X := \begin{bmatrix} \Delta \omega_1 & \Delta \omega_2 & \Delta P_{m_{1,1}} & \Delta P_{m_{1,2}} & \Delta P_{m_{2,1}} & \Delta P_{m_{2,2}} & \Delta P_{agc_1} \\ \Delta P_{agc_2} & \Delta P_{AC1,2} & \Delta P_{DC1,2} & \Delta P_{ESS_1} & \Delta P_{ESS_2} \end{bmatrix}^T, \\ d = \begin{bmatrix} \Delta P_{L_1} & \Delta P_{L_2} \end{bmatrix}^T.$$

Besides, A_c is the system matrix and $B_{c,d}$ is the input matrix. Overall, in the two-area AC/DC system which has two ESS controllers, there are three new state variables ($\Delta P_{DC1,2}$, ΔP_{ESS_1} and ΔP_{ESS_2}) of synchronous controllers that would be added, compared with a pure two-area AC system. In addition to (10), we can also derive an output model where the wide-area frequency and AC/DC power flow measurements are available to the grid operators,

$$Y(t) = CX(t), \quad (11)$$

where $Y \in \mathbb{R}^{n_y}$ represents the system output and C is the output matrix. For the purpose of numerical analysis, (10) and (11) need to be discretized. To obtain the analytical solution for the discretization, the matrices A and B_d of sampled discrete-time model with a sampling-period T_s become [19],

$$A = e^{A_c T_s}, \quad B_d = \int_{t=0}^{T_s} e^{A_c(T_s-t)} B_{c,d} dt. \quad (12)$$

III. FDI ATTACKS ON THE HYBRID AC/DC GRID

From the description above, the hybrid AC/DC grid with virtual inertia is operated by controllers (e.g., derivative control for inertia emulation, damping control for the DC link and AGC control for load-generation imbalance). These controllers collect measurements as inputs and send commands to the grid components through communication networks. As discussed in Section I, this process may make the hybrid grid exposed to cyber intrusions. In this article, we consider a high level of control and security that the FDI attacks may manipulate the system measurements of frequencies and power flows.

A. FDI attack basics: vulnerability and impact

An FDI attack can modify the system measurements to a lower or higher value. Thus the system output model under FDI attacks in discrete-time can be described by,

$$\tilde{Y}[k] = CX[k] + f[k], \quad (13)$$

where $\tilde{Y}[\cdot]$ is the corrupted output and $f[\cdot]$ denotes FDI attacks. In this article, we mainly consider the general “stationary” FDI attack where it occurs as a constant bias injection f at an unknown time instance k_{min} . Other scenarios such as scaling, ramp, pulse and random attacks are referred to [14]. These corruptions system outputs would also affect the dynamics of the hybrid grid. For instance, an attack on the AC power flow measurement between Areas i and j , say $f_{ACi,j}$, can manipulate both the SPMC control and the AGC control loops.

Thus this attack can change (5) and (8) into the following equations respectively,

$$\begin{aligned}\Delta P_{DC_{ref}} &= K_i \Delta \omega_i + K_j \Delta \omega_j + K_{AC} (\Delta P_{AC_{i,j}} + f_{AC_{i,j}}), \\ ACE_i &= \frac{\beta_i}{2\pi} \Delta \omega_i + (\Delta P_{AC_{i,j}} + f_{AC_{i,j}} + \Delta P_{DC_{i,j}}).\end{aligned}$$

Thus the state equation under FDI attacks in the discrete-time mode can be expressed as,

$$X[k+1] = AX[k] + B_d d[k] + B_f f[k], \quad (14)$$

where the matrix B_f relates FDI attacks to the system states. Note B_f is obtained through the same matrix transformation as B_d in (12), while the matrix $B_{c,f}$ in the continuous system model depends on the specific attack scenario.

Remark III.1 (Vulnerability of different system models under FDI attacks). *Consider the following system models under FDI attacks,*

- normal AC system,
- hybrid AC/DC system,
- hybrid AC/DC system with virtual inertia.

We can see that, different from the pure AC system, the hybrid AC/DC grid with virtual inertia would have more vulnerable points to FDI attacks. Intruders can manipulate the measurements of frequencies and both AC and DC power flows. Besides, according to the high-level control structure, corruptions on these measurements can affect all the controllers implemented in the hybrid AC/DC grid. In Section V-B we would present such a detailed analysis.

An intelligent FDI attacker also considers the impact of various attack strategies. The frequency properties that can be influenced by the attacker are mainly maximum (center-of-inertia) frequency deviation (MFD) or steady-state frequency deviation (SSFD). In this article, we use the former MFD as the attack impact index. The attacker may be able to trigger load shedding or generator tripping schemes by causing a large MFD. Intuitively, for a univariate FDI attack where only one measurement is compromised, a larger constant injection is more desired to cause the maximum damage. In Figure 3, we can see that with the increase of the attack value, the MFD becomes larger. To trigger load shedding schemes in the hybrid AC/DC grid with virtual inertia, the univariate attack value should be a minimum of 0.44 p.u. (while it is 0.52 p.u. in the AC/DC grid without inertia emulation capability).

B. Disruptive stealthy FDI attack strategies

The univariate attack for a large impact in Figure 3 may be detectable since it may go beyond possible thresholds and trigger data quality alarms. An advanced attack should attend to pursue a desired impact and also satisfy the undetectability criterion [20]. For that purpose, the attacker is required to have vast attack resources to manipulate multiple data channels (i.e. multivariate attacks) and enough knowledge of the targeted system operations (e.g., AGC control, HVDC coordination, inertia emulation and also data quality checking programs). Then the attacker can select “appropriate” injection values. The vulnerability of the hybrid grid to such attacks can be

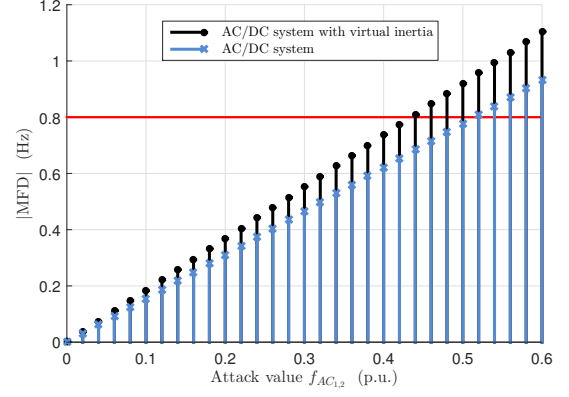


Figure 3: Attack impact: MFD of Area 1 under various values of a univariate attack $f_{AC_{1,2}}$.

quantified by computing the attack resources needed by the attacker to achieve the targets both on impact and undetectability, which is formalized in the following definition.

Definition III.2 (Vulnerability to disruptive stealthy attacks). *Consider an FDI attack with f . We call it a disruptive stealthy attack if f takes values from the set*

$$\mathcal{F} := \{f \in \mathbb{R}^{n_y} : \mathbf{b}_{\min} \leq \mathbf{F}_f f \leq \mathbf{b}_{\max}\}, \quad (15)$$

where the vectors $\mathbf{b}_{\min}, \mathbf{b}_{\max} \in \mathbb{R}^{n_b}$ and the matrix $\mathbf{F}_f \in \mathbb{R}^{n_b \times n_y}$ are scenario specific. The following Remark III.3 shows that the choice of $\mathbf{b}_{\min}, \mathbf{b}_{\max}, \mathbf{F}_f$ may be adjusted according to different national grid code. Thus, to describe the vulnerability of hybrid grids to FDI attacks, one can formulate an optimization program to compute the needed attack resources,

$$\begin{aligned}\alpha_i^* &= \min_f \|f\|_0 \\ \text{s.t. } & f \in \mathcal{F}, \quad f(i) = \mu, \\ & f(j) = 0, \quad \text{for all } j \in \mathcal{P}.\end{aligned} \quad (16)$$

where $\|\cdot\|_0$ denotes the zero vector norm, $f(i)$ is the injection with value μ on a specific measurement that the attacker can access. We also add the constraint that the protected data channels (in set \mathcal{P}) cannot be attacked. The hybrid AC/DC power grid is more vulnerable to the attack with a smaller α_i^* as it requires fewer data channels to be manipulated to achieve its targets on attack impact and undetectability.

The optimization program (16) is NP-hard. We can use the big M method to express (16) as a mixed integer linear program which can be solved by appropriate solvers. We omit details and refer to [10] for a similar reformulation.

Remark III.3 ($\mathbf{b}_{\min}, \mathbf{b}_{\max}$ and \mathbf{F}_f selection for disruptive stealthy attacks). *For an effective attack strategy, the selection of parameters $\mathbf{b}_{\min}, \mathbf{b}_{\max}$ and \mathbf{F}_f in (15) are critical. To be precise, the disruptive stealthy attacks need to satisfy the following criteria [13], [14],*

- To avoid triggering data quality alarms, the frequency deviation after corruptions should remain within a range,

$$\Delta \omega_{\min} \leq \Delta \omega_{i,f} \leq \Delta \omega_{\max},$$

- (ii) The calculated ACE of Area i during attacks $ACE_{i,f}$ should not exceed a permitted value,

$$|ACE_{i,f}| \leq ACE_{max},$$

- (iii) Similarly, the computed power reference signal for the HVDC link under FDI attack $\Delta P_{DC_{ref,f}}$ should not exceed an acceptable value,

$$|\Delta P_{DC_{ref,f}}| \leq \Delta P_{DC_{ref,max}},$$

- (iv) If the attacker targets on under-frequency load shedding or over-frequency generation tripping schemes, the MFD after corruptions should be larger than a particular value.

It is worth mentioning that the limits of (i) - (iv) are system dependent as reflected in national grid code. In this article, the values $\Delta\omega_{min}$, $\Delta\omega_{max}$, ACE_{max} and $\Delta P_{DC_{ref,max}}$ are set to be -0.1 Hz, 0.1 Hz, 0.05 p.u. and 0.1 p.u. respectively, according to [21]–[24]. To avoid load shedding, the maximum frequency deviation is defined as -0.8 Hz from the grid code in [25].

IV. ATTACK DETECTION, ISOLATION AND RECOVERY

For the hybrid system described in the state-space representation, we first show that it is a particular case of the general DAE model. Consider a time-shift operator q that $qx[k] \rightarrow x[k+1]$. We can reformulate (13) (14) into,

$$H(q)x[k] + L(q)y[k] + F(q)f[k] = 0, \quad (17)$$

where $x := [X^T d^T]^T$ contains all the unknown signals of states and disturbances, $y := \tilde{Y}$ denotes the available system output for a detector. Let n_x , n_y and n_r be the dimension of $x[\cdot]$, $y[\cdot]$ and the row number of (17). Here $H(\cdot)$, $L(\cdot)$ and $F(\cdot)$ are polynomial matrices in terms of q such that

$$H(q) := \begin{bmatrix} -qI + A & B_d \\ C & 0 \end{bmatrix}, \quad L(q) := \begin{bmatrix} 0 \\ -I \end{bmatrix}, \quad F(q) := \begin{bmatrix} B_f \\ I \end{bmatrix}.$$

A. FDI attack detector construction

The principle of an FDI attack detector is to generate a diagnosis signal to reveal the presence of the attack, giving the available data $y[k]$. Definition IV.1 characterizes its task.

Definition IV.1 (FDI attack detection). *The diagnosis signal from the detector differentiates whether the system output is a consequence of the normal disturbance or FDI attacks. Thus ideally it relates a non-zero mapping from the attack to the diagnosis signal, while it is decoupled from the effects of unknown system states and disturbances.*

In this article, we restrict the attack detector to a type of residual generator with linear transfer operations [26], i.e., $r[k] := R(q)y[k]$, where $r[\cdot]$ is called the residual signal for diagnosis, $R(q)$ is the transfer function that needs to be designed. We propose a formulation of $R(q) := a(q)^{-1}N(q)L(q)$. Now the task of detector construction comes to the design of $N(q)$ whose dimension and predefined order are n_r and d_N , if the denominator $a(q)$ with sufficient order is determined. Multiplying the left of (17) by $a(q)^{-1}N(q)$ would lead to

$$\begin{aligned} r[k] &= a(q)^{-1}N(q)L(q)y[k] \\ &= -\underbrace{a(q)^{-1}N(q)H(q)x[k]}_{(I)} - \underbrace{a(q)^{-1}N(q)F(q)f[k]}_{(II)}. \end{aligned} \quad (18)$$

Term (I) is the part from the effect of unknown system states and disturbances $x[\cdot]$. Term (II) corresponds to the FDI attack. Thus according to Definition IV.1, the desired detector would generate the residual signal $r[\cdot]$ that can be decoupled from $x[\cdot]$ but keep sensitive to $f[\cdot]$. We would expect

$$N(q)H(q) = 0, \quad N(q)F(q) \neq 0. \quad (19)$$

Inspired by (19), the following theoretical result shows an effective way for attack detection and also recovery.

Theorem IV.2 (FDI attack detection and recovery). *It can be observed that $H(q) = \sum_{i=0}^1 H_i q^i$, $N(q) := \sum_{i=0}^{d_N} N_i q^i$ and $F(q) = F$. Consider an FDI attack in the set (15), a residual generator with the following linear program characterizations for (19) can have non-zero residual output that recovers the attack value f in the steady-state behavior,*

$$\begin{cases} \bar{N}\bar{H} = 0, \\ -a(1)^{-1} \sum_{i=0}^{d_N} N_i F = 1, \end{cases} \quad (20)$$

where the matrices \bar{N} , \bar{H} are defined as

$$\bar{N} := \begin{bmatrix} N_0 & N_1 & \cdots & N_{d_N} \end{bmatrix},$$

$$\bar{H} := \begin{bmatrix} H_0 & H_1 & 0 & \cdots & 0 \\ 0 & H_0 & H_1 & 0 & \vdots \\ \vdots & 0 & \ddots & \ddots & 0 \\ 0 & \cdots & 0 & H_0 & H_1 \end{bmatrix}.$$

Proof. Note that $N(q)H(q) = \bar{N}\bar{H}[I, qI, \dots, q^{d_N+1}I]^T$. If $\bar{N}\bar{H} = 0$ as stated in (20), the diagnosis filter becomes $r[k] = -a(q)^{-1}N(q)f[k]$. The steady-state value of the residual signal under the FDI attack would become $-a(q)^{-1}N(q)F(q)f \mid_{q=1}$. To track the FDI attack magnitude, one can simply make $-a(1)^{-1}N(1)F(1) = 1$. Due to that $N(1)F(1) = \sum_{i=0}^{d_N} N_i F$, the residual signal from (20) recovers the exact attack value f in the steady state behavior. ■

Next, the residual generator design becomes to find a feasible \bar{N} satisfying (20). To increase the sensitivity of the residual generator to the attack, in addition to (20), the detector may also aim to let the coefficients of $N(q)F(q)$ in (19) achieve the maximum value. We then reformulate the attack detection and recovery problem as the optimization program,

$$\begin{aligned} \gamma^* &= \max_{\bar{N}} \quad \|\bar{N}\bar{F}\|_{\infty} \\ \text{s.t.} \quad & \bar{N}\bar{H} = 0, \quad \|\bar{N}\|_{\infty} \leq \eta, \\ & -a(1)^{-1} \sum_{i=0}^{d_N} N_i F = 1. \end{aligned} \quad (21)$$

where the constraint $\|\bar{N}\|_{\infty} \leq \eta$ is added to avoid possible unbounded solutions and it does not affect the performance of the detector. The matrix \bar{F} has a similar definition with \bar{H} in Theorem IV.2. To be precise, the proposed optimization program (21) is not a linear program (LP) due to the non-convex objective function. However, as explained by a similar argument in [27, Lemma 4.3], one can view (21) as a family of n standard LPs where n is the number of columns of \bar{F} .

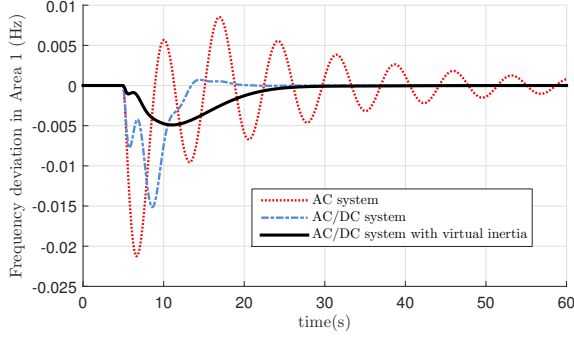


Figure 4: Frequency responses of Area 1 under load changes.

Remark IV.3 (Attack isolation). *The residual generator from (21) is mainly designed for one univariate attack. For multivariate intrusions ($\alpha_i^* > 1$ from (16)), an alternative is to build a bank of residual generators where each of them aims to detect one particular intrusion and keep insensitive to others, by considering the following “reconstructed” DAE,*

$$\begin{bmatrix} \mathbf{H}(q) & \mathbf{F}_{-j}(q) \end{bmatrix} \begin{bmatrix} \mathbf{x}[k] \\ \mathbf{f}_{-j}[k] \end{bmatrix} + \mathbf{L}(q)\mathbf{y}[k] + \mathbf{F}_j(q)\mathbf{f}_j[k] = 0, \quad (22)$$

where $\mathbf{F}_{-j}(q)$ is the polynomial matrix that includes all columns of $\mathbf{F}(q)$ except the j -th one, and similarly $\mathbf{f}_{-j}[k]$ contains all the elements of $\mathbf{f}[k]$ except the j -th one. Then the j -th residual generator can be designed using the same approach in Theorem IV.2 and (21) for the j -th intrusion while isolating the effects from others. The j -th intrusion can be identified by the j -th residual generator since the other residual generators keep insensitive to this intrusion. Besides, with (21), it can recover the j -th attack’s value in the steady-state behavior. Similar lines of such arguments can be found in [13, Section V.B].

Remark IV.3 shows that the attack isolation problem can be treated as an attack detection task effectively. In the end, we provide sufficient and necessary conditions for the feasibility of attack detection and isolation,

Lemma IV.4 (Necessary and sufficient condition of detectability and isolability). *For a single FDI attack ($\alpha_i^* = 1$), it is detectable that satisfies (19) if, and only if,*

$$\text{Rank} \left(\begin{bmatrix} \mathbf{H}(q) & \mathbf{F}(q) \end{bmatrix} \right) > \text{Rank} (\mathbf{H}(q)). \quad (23)$$

Besides, for multivariate FDI attacks ($\alpha_i^ > 1$), one particular intrusion \mathbf{f}_j is isolable from others if, and only if,*

$$\text{Rank} \left(\begin{bmatrix} \mathbf{H}(q) & \mathbf{F}(q) \end{bmatrix} \right) > \text{Rank} \left(\begin{bmatrix} \mathbf{H}(q) & \mathbf{F}_{-j}(q) \end{bmatrix} \right). \quad (24)$$

Proof. The detectability condition (23) is adapted from [12, Theorem 3]. Alternatively, (23) can be rewritten as $\mathbf{F}(q) \notin \text{Im}(\mathbf{H}(q))$. It ensures that while the unknown system states and disturbances are decoupled, the residual signal keeps sensitive to the FDI attack. For the isolability criterion, note that $\mathbf{H}(q)$ in the form of (17) can be replaced by $\begin{bmatrix} \mathbf{H}(q) & \mathbf{F}_{-j}(q) \end{bmatrix}$ in (22) of Remark (IV.3). The condition (22) can be also rewritten as $\mathbf{F}_j(q) \notin \text{Im}(\begin{bmatrix} \mathbf{H}(q) & \mathbf{F}_{-j}(q) \end{bmatrix})$. ■

V. NUMERICAL RESULTS

A. Preliminaries for simulations

In order to evaluate the vulnerability and impact of the hybrid AC/HVDC grid to FDI attacks, and also validate the effectiveness of the proposed attack detection methodology, in this section, we study the two-area interconnected AC/DC system and provide numerical results. As shown in Figure 1, there are two GENs and one load demand center in each area. The system parameters of the two-area grid with parallel AC/DC lines and ESS for virtual inertia and the control parameters of this case study are referred to [18]. Given the characterizations of time responses of controllers, the sampling period T_s is given as 0.2s. We can obtain a 12-order discrete-time model which can be fitted into the form of (17).

In the detector design, the degree of the residual generator is set to $d_N = 3$ which is much less than the order of the system. Besides, we give the denominator a formulation of $\mathbf{a}(q) = (q - p)^{d_N} / (1 - p)^{d_N}$ where p can be treated as the pole of $R(q)$, and it is normalized in steady-state value for all feasible poles [26]. All the optimization programs are solved in CPLEX.

B. Vulnerability of hybrid systems to FDI attacks

First, we present the result of frequency deviations under normal conditions in Figure 4 where the system input is only one step load change ($\Delta P_{L1} = 0.03$ p.u. at $t = 5$ s). The comparisons are made on the normal AC system, hybrid AC/DC system and hybrid AC/DC system with virtual inertia. We can see that the HVDC link and especially, the inertia emulation, can improve the system dynamics significantly in damping frequency oscillations, which proves the effectiveness of the high-level control strategy of this article.

Next, in order to evaluate the vulnerability of different system models under FDI attacks, we launch univariate attacks on the wide-area system frequency and AC/DC power flow measurements separately (recall Figure 1 for vulnerable points). The simulation results are presented in Figure 5. In all scenarios, the univariate attack with the same attack value can cause the most severe “damage” to the hybrid AC/DC system with virtual inertia. Comparing with the normal AC system and the system with parallel AC/DC lines but without virtual inertia, the AC/DC system with virtual inertia capability is with the largest MFDs under each FDI attack. This observation is consistent with Remark III.1. In fact, as stated in Remark III.1, corruptions on the frequencies and AC/DC power flows would affect all the control operations (AGC, SPMC and inertia emulator) as they are inputs to these controllers in our high-level control structure.

We continue with disruptive stealthy attacks introduced in Section III-B. These attacks can be multivariate to achieve the targets on attack impact and undetectability, and are obtained by solving the optimization program (16) for vulnerability analysis. From the results of (16), a multivariate FDI attack ($\alpha_i^* = 2$) that can manipulate both AC and DC power lines with $f_{AC1,2} = 0.44$ p.u. and $f_{DC1,2} = -0.39$ p.u. is a disruptive stealthy attack in the set of (15) for the hybrid AC/DC grid with virtual inertia. Figure 6 shows the frequency response of Area 1 under this multivariate attack. The MFD reaches -0.8 Hz at

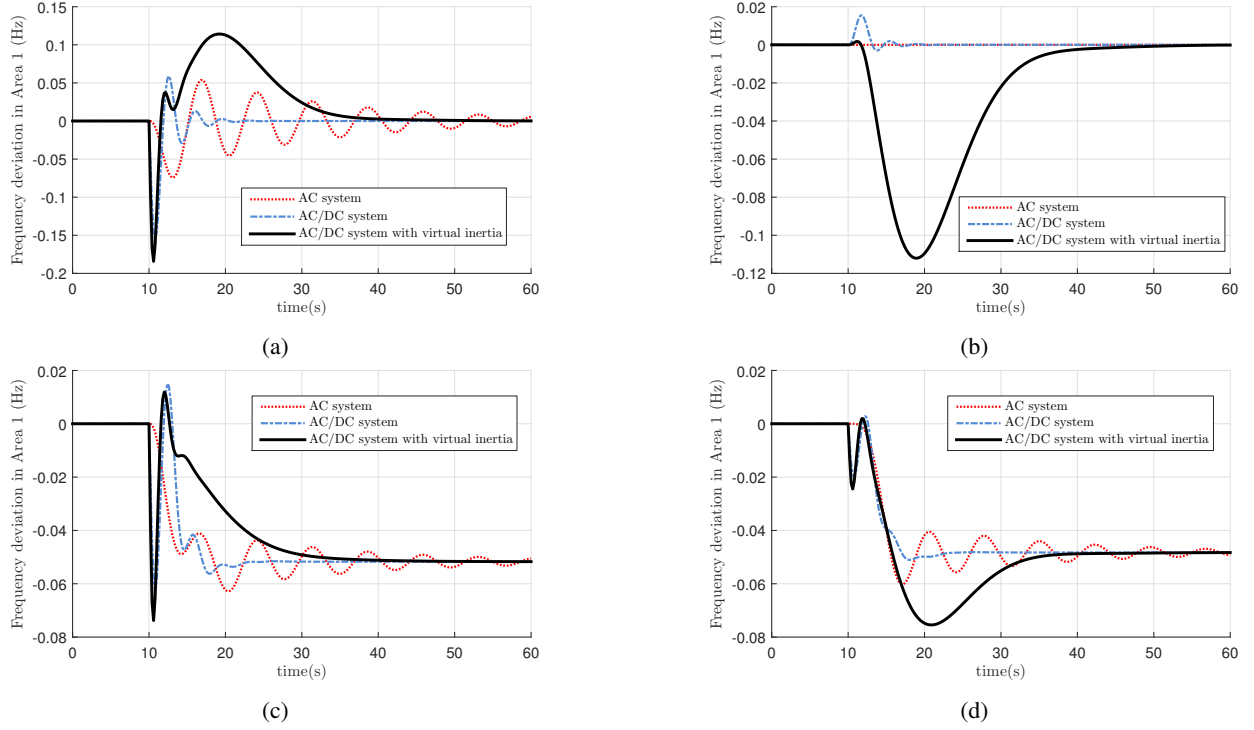


Figure 5: Frequency responses of Area 1 under univariate attacks (a) on AC line, $f_{AC1,2} = 0.1$ p.u.. (b) on DC line, $f_{DC1,2} = 0.1$ p.u.. (c) on frequency of Area 1, $f_{\omega_1} = 0.1$ Hz. (d) on frequency of Area 2, $f_{\omega_2} = 0.1$ Hz.

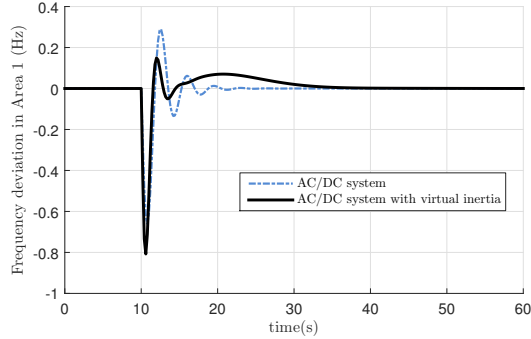


Figure 6: Frequency responses of Area 1 under multivariate attack on both AC and DC links.

around $t = 11$ s while the attack is launched at $t = 10$ s, possibly triggering load shedding schemes. The MFD of the AC/DC grid without virtual inertia has not reached -0.8 Hz yet under the same multivariate attack. To be noted, there is no disruptive stealthy attack in the type of Definition III.2 when solving (16) for the normal AC system. Thus it can be concluded that the hybrid AC/DC grids are more vulnerable to FDI attacks.

C. FDI attack detection and recovery

In the third simulations, we validate the proposed methodology of attack detection, isolation and recovery. To challenge the detector, the disturbance \mathbf{d} is modeled as stochastic load patterns; see Figure 7a of ΔP_{L_1} . The adversarial cases come from the disruptive stealthy attacks obtained in the above section. We build a bank of two residual generators to detect

and isolate the attacks $f_{AC1,2}$ and $f_{DC1,2}$ on the hybrid AC/DC grid with virtual inertia, using the approach in Remark IV.3 and (21). The optimal values of (21) achieve $\gamma^* = 4.440$ in the residual generator construction for $f_{AC1,2}$ and $\gamma^* = 2.649$ for $f_{DC1,2}$, which implies a successful detection and isolation as indicated by Lemma IV.4.

In Figure 7, the results of the residual generators under disturbances and attacks are presented. Both detectors have generated a residual signal for the presence of FDI attacks in the multivariate intrusions. Besides, we can also see that the resulted residual generators with designed capability in Theorem IV.2 can recover the exact attack values; see the steady-state residual values in Figure 7b and Figure 7c are equal to 0.44 p.u. and -0.39 p.u.. The residual signals are also decoupled from each other and stochastic load changes. Next, to test the residual generators in a more realistic setting, we also provide the simulation results where there exist noises in the process and measurements of the hybrid grid. Zero-mean Gaussian noises with the covariance 0.0009 to the frequency and 0.03 to the other states [13]. Figure 7d shows one instance of the residual signals for and it still works effectively in detecting and tracking the attack values. In the end, it should be mentioned that in these simulations the pole of $a(q)$ is set to be $p = 0.1$ for a fast response of the residual generator. If it is set to be larger to close to 1, the residual generator would respond slower but become more insensitive to noises, according to the role of p in the transfer function.

VI. CONCLUSION

In this article, we investigated FDI attacks on the hybrid AC/DC grid with virtual inertia. Our study shows that the

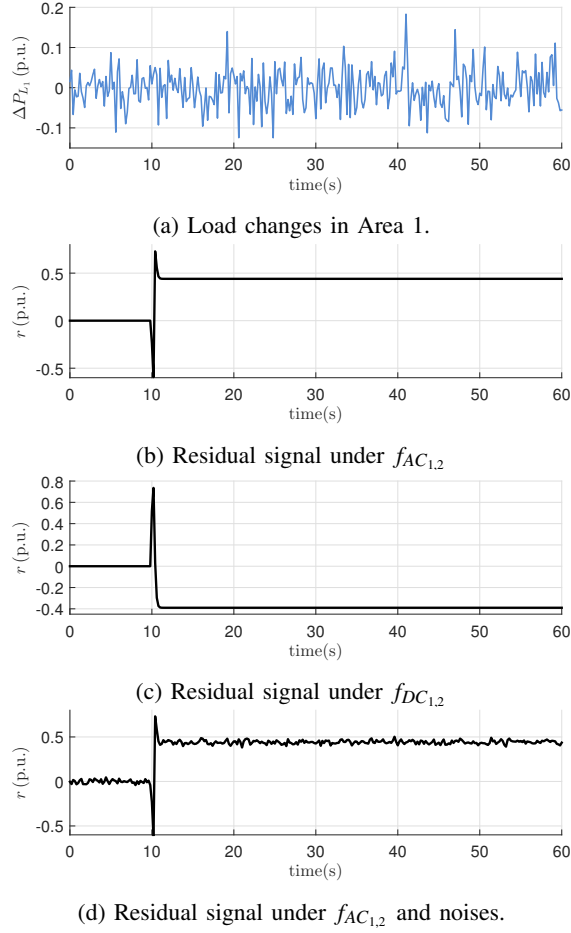


Figure 7: Residual responses under multivariate attacks.

hybrid grid can be more vulnerable to attacks. We offer a vulnerability and impact analysis framework to study that on the hybrid AC/DC grids. We also propose a powerful tool to detect, isolate and recover all the intrusions. The effectiveness of these methods was validated by simulations in the AC/DC interconnected two-area system. The future research includes the study of other types of attacks on the hybrid grids and a special focus on the vulnerability of different inertia emulation strategies to these attacks.

REFERENCES

- [1] E. Rakhshani, D. Remon, and P. Rodriguez, "Effects of pll and frequency measurements on lfc problem in multi-area hvdc interconnected systems," *International Journal of Electrical Power & Energy Systems*, vol. 81, pp. 140–152, 2016.
- [2] T. Xu, W. Jang, and T. Overbye, "Commitment of fast-responding storage devices to mimic inertia for the enhancement of primary frequency response," *IEEE Transactions on Power Systems*, vol. 33, no. 2, pp. 1219–1230, Mar. 2018.
- [3] C. Mosca, F. Arrigo, A. Mazza, E. Bompard, E. Carpaneto, G. Chicco, and P. Cuccia, "Mitigation of frequency stability issues in low inertia power systems using synchronous compensators and battery energy storage systems," *IET Generation, Transmission & Distribution*, vol. 13, no. 17, pp. 3951–3959, 2019.
- [4] G. Liang, S. R. Weller, J. Zhao, F. Luo, and Z. Y. Dong, "The 2015 Ukraine blackout: Implications for false data injection attacks," *IEEE Trans. on Power Syst.*, vol. 32, no. 4, pp. 3317–3318, Jul. 2017.

- [5] R. Tan, H. H. Nguyen, E. Y. S. Foo, D. K. Y. Yau, Z. Kalbarczyk, R. K. Iyer, and H. B. Gooi, "Modeling and mitigating impact of false data injection attacks on automatic generation control," *IEEE Transactions on Information Forensics and Security*, vol. 12, no. 7, pp. 1609–1624, Jul. 2017.
- [6] J. Fang, R. Zhang, H. Li, and Y. Tang, "Frequency derivative-based inertia enhancement by grid-connected power converters with a frequency-locked-loop," *IEEE Transactions on Smart Grid*, vol. 10, no. 5, pp. 4918–4927, Sep. 2019.
- [7] L. Ruttledge and D. Flynn, "Short-term frequency response of power systems with high non-synchronous penetration levels," *Wiley Interdisciplinary Reviews: Energy and Environment*, vol. 4, no. 5, pp. 452–470, 2015.
- [8] M. Datta and T. Senjyu, "Fuzzy control of distributed PV inverters/energy storage systems/electric vehicles for frequency regulation in a large power system," *IEEE Transactions on Smart Grid*, vol. 4, no. 1, pp. 479–488, Mar. 2013.
- [9] I. Dudurych, M. Burke, L. Fisher, M. Eager, and K. Kelly, "Operational security challenges and tools for a synchronous power system with high penetration of non-conventional sources," *CIGRE Science & Engineering*, no. 7, pp. 91–101, 2017.
- [10] A. Teixeira, K. C. Sou, H. Sandberg, and K. H. Johansson, "Secure control systems: A quantitative risk management approach," *IEEE Control Systems*, vol. 35, no. 1, pp. 24–45, 2015.
- [11] P. M. Esfahani, M. Vrakopoulou, K. Margellos, J. Lygeros, and G. Andersson, "Cyber attack in a two-area power system: Impact identification using reachability," in *American Control Conf.*, Jun. 2010, pp. 962–967.
- [12] M. Nyberg and E. Frisk, "Residual generation for fault diagnosis of systems described by linear differential-algebraic equations," *IEEE Trans. on Autom. Control*, vol. 51, no. 12, pp. 1995–2000, 2006.
- [13] A. Ameli, A. Hooshyar, E. El-Saadany, and A. Youssef, "Attack detection and identification for automatic generation control systems," *IEEE Transactions on Power Systems*, p. 1, 2018.
- [14] S. Sridhar and M. Govindarasu, "Model-based attack detection and mitigation for automatic generation control," *IEEE Transactions on Smart Grid*, vol. 5, no. 2, pp. 580–591, Mar. 2014.
- [15] K. Pan, A. Teixeira, M. Cvetkovic, and P. Palensky, "Cyber risk analysis of combined data attacks against power system state estimation," *IEEE Transactions on Smart Grid*, p. 1, 2018.
- [16] R. Fan, J. Lian, K. Kalsi, and M. Elizondo, "Impact of cyber attacks on high voltage dc transmission damping control," *Energies*, vol. 11, no. 5, p. 1046, 2018.
- [17] A. Gholami, M. Mousavi, A. K. Srivastava, and A. Mehrizi-Sani, "Cyber-physical vulnerability and security analysis of power grid with hvdc line," in *2019 North American Power Symposium (NAPS)*, Wichita, Kansas, 2019, pp. 1–6.
- [18] E. Rakhshani and P. Rodriguez, "Inertia emulation in AC/DC interconnected power systems using derivative technique considering frequency measurement effects," *IEEE Transactions on Power Systems*, vol. 32, no. 5, pp. 3338–3351, Sep. 2017.
- [19] K. Ogata, *Discrete-time Control Systems (2Nd Ed.)*. Upper Saddle River, NJ, USA: Prentice-Hall, Inc., 1995.
- [20] C. Chen, K. Zhang, K. Yuan, L. Zhu, and M. Qian, "Novel detection scheme design considering cyber attacks on load frequency control," *IEEE Transactions on Industrial Informatics*, vol. 14, no. 5, pp. 1932–1941, 2018.
- [21] P. Kundur, N. Balu, and M. Lauby, *Power System Stability and Control*, ser. Discussion Paper Series. McGraw-Hill Education, 1994. [Online]. Available: <https://books.google.nl/books?id=2cbvyf8Ly4AC>
- [22] H. Weng and Z. Xu, "Wams based robust hvdc control considering model imprecision for ac/dc power systems using sliding mode control," *Electric Power Systems Research*, vol. 95, pp. 38–46, 2013.
- [23] ENTSO-E, "Frequency stability evaluation criteria for the synchronous zone of continental europe," ENTSO-E, Tech. Rep., 2016.
- [24] J. Garcia, K. Mudunkotuwa, and C. Shumski, "Migrate project – type-3 and type-4 emt model documentation," Manitoba HVDC Research Centre, Winnipeg, Tech. Rep., 2017.
- [25] ENTSO-E, "Continental europe operation handbook, policy 1: Load-frequency control and performance – appendix," ENTSO-E, Brussels, Belgium, Tech. Rep., Mar. 2016.
- [26] K. Pan, P. Palensky, and P. M. Esfahani, "From static to dynamic anomaly detection with application to power system cyber security," *IEEE Transactions on Power Systems*, pp. 1–1, 2019.
- [27] P. M. Esfahani and J. Lygeros, "A tractable fault detection and isolation approach for nonlinear systems with probabilistic performance," *IEEE Trans. on Autom. Control*, vol. 61, no. 3, pp. 633–647, Mar. 2016.